

An Analytical Approach to Sound Field Reproduction Using Circular and Spherical Loudspeaker Distributions

Jens Ahrens, Sascha Spors

Quality and Usability Lab, Deutsche Telekom Laboratories, Technische Universität Berlin, Ernst-Reuter-Platz 7, 10587 Berlin, Germany. {jens.ahrens,sascha.spors}@telekom.de

Summary

In this paper, we present the theoretical basics and implementation strategies for sound field reproduction using circular and spherical loudspeaker arrays. The presented approach can be seen as an analytical formulation of what is known as higher order Ambisonics. It relies on the assumption of a continuous distribution of secondary sources on which sampling is performed to yield the loudspeaker driving signals for real-world implementations. We present the theoretical derivation of the loudspeaker driving signals and investigate the properties of the actual reproduced wave field, whereby the focus lies on the consequences of the spatial discretization of the secondary source distribution.

PACS no. 43.38.Md, 43.60.Fg, 43.60.Sx, 43.60.Tj

1. Introduction

Since several decades, the problem of physically recreating a given wave field has been addressed in the audio community. It turned out that two alternative approaches exist. The first of these approaches bases on the straightforward solution of the reproduction equation for the loudspeaker driving signals. The alternative is known as wave field synthesis (WFS), e.g. [1], and is directly derived from the Kirchhoff-Helmholtz integral equation.

In this article we concentrate on the former. The best-known representative of these approaches is Ambisonics [2]. The desired wave field is typically described via its spatial harmonics expansion coefficients [3]. These can be yielded either from appropriate microphone recording techniques [4] (data-based reproduction) or virtual sound scenes may be composed of virtual sound sources whose spatial harmonics expansion coefficients are derived from analytical source models (model-based reproduction).

The original Ambisonics approach [3] is based on the assumption of a finite number of discrete loudspeakers whose emitted wave fields superpose to an approximation of the desired one. Typically, numerical algorithms are employed to find the appropriate loudspeaker driving signals.

Besides Ambisonics alternative formulations like [5, 6, 7, 8] exist which all follow a similar strategy. The difference between these proposals is mainly the numerical algorithm which solves the employed equation system. However, we are aware that this is a disputable question.

Some of the above mentioned approaches of the first type, especially [5, 6, 8], are principally not limited to specific loudspeaker setups. However, their formulation does not exploit any a priori knowledge of the actual loudspeaker setup giving away the potential to reduce computational complexity. The computational complexity is generally very high in [3, 7, 5, 6, 8] due to the numerical algorithms employed.

As outlined by the authors in [9], the theoretical basis for the presented work is the so-called simple source approach [10] which has gained only little attention in conjunction with sound field reproduction so far. An equivalent formulation has been published in parallel in [11].

Wave-field synthesis, the alternative to the above mentioned approaches, e.g. [1], employs a modified formulation of the Kirchhoff-Helmholtz integral to determine the loudspeaker driving signals. Numerous attempts of comparing the two alternatives have been made during the years, e.g. [12]. However, the results are rather unsatisfying, mostly due to the fact that Ambisonics and its relatives rely on a discrete formulation, wave field synthesis on a continuous one. The presented approach constitutes a significant step towards an analytical comparison as performed in [13].

A comparative numerical study of a selection of sound field reproduction approaches can be found in [14] which shows that all investigated methods perform comparably in terms of accuracy. It can not be expected to significantly gain accuracy in the reproduction employing an analytical formulation. However, as noted above, there is indeed potential to reduce the computational complexity. Furthermore, contrary to the analytical method presented in this

paper, numerical methods such as [3, 5, 6, 7, 8] give only little insight into the general properties of the reproduced wave field.

1.1. Nomenclature

The following notational conventions are used: For scalar variables lower case denotes the time domain, upper case the temporal frequency domain. Vectors are denoted by lower case boldface. The three-dimensional position vector in Cartesian coordinates is given as $\mathbf{x} = [x \ y \ z]^T$. The Cartesian coordinates are linked to the spherical coordinates via $x = r \cos \alpha \sin \beta$, $y = r \sin \alpha \sin \beta$, and $z = r \cos \beta$. α denotes the azimuth, β the elevation. Confer also to Figure 1. For functions dependent on spatial coordinates, we use the notations $F(\mathbf{x})$ respectively $F(r, \alpha, \beta)$ to emphasize a given coordinate system.

The acoustic wavenumber is denoted by k . It is related to the temporal frequency by $k^2 = (\omega/c)^2$ with ω being the radial frequency and c the speed of sound. Propagating monochromatic plane waves and outgoing spherical waves are denoted by $e^{-i\mathbf{k}_{pw}^T \mathbf{x}}$ and $(1/r)e^{-ir\omega/c}$ respectively, with $\mathbf{k}_{pw}^T = (\omega/c)[\cos \theta_{pw} \sin \phi_{pw} \ \sin \theta_{pw} \sin \phi_{pw} \ \cos \phi_{pw}]^T$ and (θ_{pw}, ϕ_{pw}) denoting the propagation direction of the plane wave. i is the imaginary unit ($i = \sqrt{-1}$).

Due to the continuous formulation, we will not refer to loudspeakers but rather to secondary sources respectively their distributions and also to secondary source driving functions rather than to loudspeaker signals.

The term driving function as referred to in this paper, denotes the function $D(\omega)$ by which an input signal $\hat{S}(\omega)$ has to be filtered to yield the secondary source driving signal $S_D(\omega)$. In the temporal frequency domain this formulation reads

$$S_D(\omega) = \hat{S}(\omega) \cdot D(\omega). \quad (1)$$

We occasionally refer to *two-dimensional* wave fields. In this case a given wave field $P(\mathbf{x}, \omega)$ is independent of one of the spatial coordinates, so that e.g. $P(x, y, z, \omega) = P(x, y, \omega)$.

1.2. Mathematical preliminaries

In this paper, we exclusively treat monochromatic steady-state wave fields, thus

$$P(\mathbf{x}, \omega) = P(\mathbf{x}, \omega) \cdot 2\pi\delta(\omega - \omega_0), \quad (2)$$

with $\delta(\cdot)$ denoting the Dirac delta function. The broadband driving function as used in (1) is yielded by evaluating the monochromatic driving function for different frequencies over the desired bandwidth.

Due to the sifting property of the Dirac delta function [15], $P(\mathbf{x}, \omega)$ on the right-hand side of (2) can be written as $P(\mathbf{x}, \omega_0)$ and the transformation of (2) to the time domain reads

$$p(\mathbf{x}, t) = P(\mathbf{x}, \omega_0) \cdot e^{i\omega_0 t}. \quad (3)$$

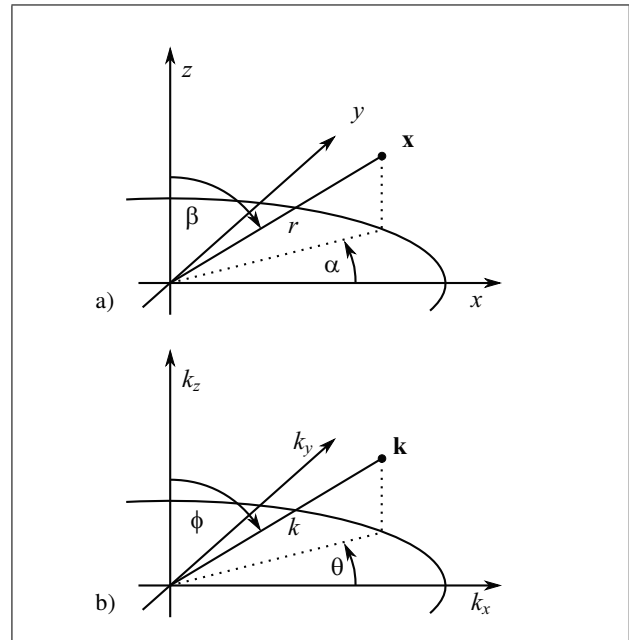


Figure 1. The coordinate systems used in this paper. a) Spatial domain, b) Wave number domain.

We therefore do not explicitly consider the time domain since $P(\mathbf{x}, \omega_0)$ already contains all information. We use complex notation for harmonic signals. When wave fields are illustrated in figures, only the real part is depicted.

A propagating wave field can be described by its spherical harmonics expansion as [10]

$$F(\mathbf{x}, \omega) = \sum_{n=0}^{\infty} \sum_{m=-n}^n \hat{F}_n^m(r, \omega) Y_n^m(\alpha, \beta). \quad (4)$$

The expansion coefficients $\hat{F}_n^m(r, \omega)$ are

$$\hat{F}_n^m(r, \omega) = \check{F}_n^m(\omega) j_n\left(\frac{\omega}{c} r\right), \quad (5)$$

whereby $j_n(\omega r/c)$ denotes the n -th order spherical Bessel function of first kind [10].

The spherical harmonics $Y_n^m(\alpha, \beta)$ are defined as

$$Y_n^m(\alpha, \beta) = \sqrt{\frac{(2n+1)(n-m)!}{4\pi(n+m)!}} \cdot P_n^m(\cos \beta) \cdot e^{im\alpha}, \quad (6)$$

with $P_n^m(\cdot)$ denoting the m -th order associated Legendre polynomial of n -th degree.

The Fourier series expansion of a two-dimensional propagating wave field is [10]

$$F(r, \alpha, \omega) = \sum_{m=-\infty}^{\infty} \hat{F}_m^m(r, \omega) e^{im\alpha}. \quad (7)$$

2. The ambisonics approach

2.1. General outline

The term *Ambisonics* goes back to Michael Gerzon, the protagonist of the early Ambisonics years. It is Latin and literally means *surround sound* [16]. However, a clear technical definition of the approach does not exist.

In the basic three-dimensional Ambisonics approach, the loudspeakers of the respective reproduction system are located on a sphere around the listening area. Both the desired wave field as well as the sound fields emitted by the loudspeakers are expanded into series of orthogonal basis functions [2, 3]. More recent Ambisonics approaches are typically referred to as *higher order Ambisonics*. However, the term *higher order* is rather a historical rudiment. It simply emphasizes the fact that the expansions are not restricted to low (e.g. 1) expansion orders. The main motivation for concentrating on low orders is the fact that sound field recording techniques are limited to low orders (confer to sections 6.2 and 6.3).

In this paper, we describe a generic theoretical framework whose basic formulation does not take practical limitations a priori into account. We therefore waive the attribute *higher order* and implicitly speak of what is termed higher order Ambisonics, whenever we use the term Ambisonics. We comment on practical limitations wherever they arise.

The expansion of the involved wave fields into spatial basis functions allows for a mode matching procedure which leads to an equation system that is solved for the optimal loudspeaker driving signals. These drive the loudspeakers such that their superposed wave fields best approximate the desired one in a given sense,

$$P(\mathbf{x}, \omega) = \sum_{n=0}^{N-1} D(\mathbf{x}_n, r_0, \omega) \cdot G(\mathbf{x} - \mathbf{x}_n, \omega), \quad (8)$$

where $P(\mathbf{x}, \omega)$ denotes the desired wave field, $D(\mathbf{x}_n, r_0, \omega)$ the driving signal of the loudspeaker located at the position $\mathbf{x}_n = r_0 \cdot [\cos \alpha_n \sin \beta_n \sin \alpha_n \sin \beta_n \cos \beta_n]^T$, and $G(\mathbf{x} - \mathbf{x}_n, \omega)$ its spatio-temporal transfer function. Typically, numerical algorithms are employed to find the appropriate loudspeaker driving signals. These algorithms tend to be computationally costly and only little insight into the properties of the actual reproduced wave-field is gained.

The Ambisonics approach is usually divided into an encoding and a decoding stage to allow for storing and transmission of content independently from the loudspeaker setup. For ease of illustration we will skip the encoding/decoding procedure and directly derive the loudspeaker driving signals from the initial virtual wave field description. The encoding and decoding of wave fields is separately described in section 6.3.

2.2. Continuous formulation

The formulation of the basic Ambisonics equation (8) for a continuous secondary source distribution on a sphere whose center resides in the coordinate origin reads [9]

$$P(\mathbf{x}, \omega) = \int_{\Omega_0 \in S_r^2} D(\Omega_0, \omega) \cdot G(\mathbf{x} - \mathbf{x}_0, \omega) d\Omega_0, \quad (9)$$

whereby Ω_0 denotes the surface of the sphere with radius r_0 on which the secondary sources are located. \mathbf{x}_0 is a point on the sphere at

$$\mathbf{x}_0 = r_0 [\cos \alpha_0 \sin \beta_0 \sin \alpha_0 \sin \beta_0 \cos \beta_0]^T.$$

The explicit integration operation is

$$\int_{\Omega_0} d\Omega_0 = \int_0^{2\pi} \int_0^\pi r_0 \sin \beta_0 d\beta_0 d\alpha_0.$$

Note that a formulation of equation (9) for continuous linear and planar secondary source distributions can be found in [17].

When the spatial transfer function of the loudspeakers is modeled as spherical wave with flat temporal frequency response, equation (9) essentially constitutes the simple source approach for an interior problem in a spherical volume [10, 18]. In this case $G(\mathbf{x} - \mathbf{x}_0, \omega)$ can be interpreted as three-dimensional free-field Green's function.

The simple source approach for interior problems states that the acoustic field generated by events outside a volume can also be generated by a continuous distribution of secondary simple sources replacing these events and enclosing the respective volume [10]. Note that other than the Kirchhoff-Helmholtz integral equation, the simple source approach does not pose any restrictions on the wave field in locations outside of the sphere ($|\mathbf{x}| > r_0$).

A fundamental property of (9) is its inherent non-uniqueness and ill-posedness [18]. I.e. in certain situations, the solution is undefined and so-called *critical* or *forbidden frequencies* arise. These forbidden frequencies are discrete and represent the resonances of the spherical cavity. In simple words, resonances exhibit a zero on the boundary of the cavity. Since the secondary sources are positioned in these zeros, they can not excite the respective mode. However, there are indications that the forbidden frequencies are only of minor relevance when practical implementations are considered [10]. Confer also to sections 3 and 4.1.

3. Spherical secondary source distributions

In this section, we illustrate how wave field reproduction according to (9) and thus according to the simple source approach can be accomplished.

Equation (9) can be interpreted as a convolution along the surface of a sphere. In that case, the convolution theorem

$$\hat{P}_n^m(r, \omega) = 2\pi r_0 \sqrt{\frac{4\pi}{2n+1}} \hat{D}_n^m(\omega) \cdot \hat{G}_n^0(r, \omega), \quad (10)$$

and thus

$$\dot{D}_n^m(\omega) = \frac{1}{2\pi r_0} \sqrt{\frac{2n+1}{4\pi}} \frac{\dot{P}_n^m(r, \omega)}{\check{G}_n^0(r, \omega)} \quad (11)$$

applies [19]. The asymmetry of the convolution theorem (10), $\dot{P}_n^m(r, \omega)$ vs. $\check{G}_n^0(r, \omega)$ is a consequence of the definition of (9) as left convolution. An according convolution theorem for right convolutions exists [19]. Note that (10) is the analog to the mode-matching which is performed in the traditional Ambisonics approach, e.g. [3].

Introducing the explicit expression for the coefficients $\dot{P}_n^m(r, \omega)$ resp. $\check{G}_n^0(r, \omega)$ given by (5) into (11),

$$\dot{D}_n^m(\omega) = \frac{1}{2\pi r_0} \sqrt{\frac{2n+1}{4\pi}} \frac{\check{P}_n^m(\omega) \cdot j_n\left(\frac{\omega}{c}r\right)}{\check{G}_n^0(\omega) \cdot j_n\left(\frac{\omega}{c}r\right)}, \quad (12)$$

it can be seen that the parameter r appears both in the numerator as well as in the denominator in (12) in the function $j_n\left(\frac{\omega}{c}r\right)$. For $j_n\left(\frac{\omega}{c}r\right) \neq 0$, $j_n\left(\frac{\omega}{c}r\right)$ and thus r cancel out directly. For $\frac{\omega}{c}r = 0$, de l'Hôpital's rule [20] can be applied to proof that $j_n(0)$ also cancels out. The driving function is thus independent from the receiver position in these cases.

However, in particular situations, i.e. when $j_n(\omega r/c) = 0$ and $\frac{\omega}{c}r \neq 0$, (12) can be undefined. In this case forbidden frequencies arise (confer to section 2.2).

A mathematical workaround to get rid of forbidden frequencies and therefore to avoid computational instabilities in practical implementations is to reference the reproduced wave field to the center of the secondary source distribution [10]. Then all Bessel functions in (11) cancel out yielding

$$\dot{D}_n^m(\omega) = \frac{1}{2\pi r_0} \sqrt{\frac{2n+1}{4\pi}} \frac{\check{P}_n^m(\omega)}{\check{G}_n^0(\omega)}. \quad (13)$$

The secondary source driving function $D_{3D}(\alpha, \beta, \omega)$ for three-dimensional reproduction of a desired wave field with expansion coefficients $\check{P}_n^m(\omega)$ is then

$$D_{3D}(\alpha, \beta, \omega) = \frac{1}{2\pi r_0} \sum_{n=0}^{\infty} \sum_{m=-n}^n \sqrt{\frac{2n+1}{4\pi}} \frac{\check{P}_n^m(\omega)}{\check{G}_n^0(\omega)} Y_n^m(\alpha, \beta). \quad (14)$$

The coefficients $\check{P}_n^m(\omega)$ resp. $\check{G}_n^0(\omega)$ can be found in Table I for a selection of analytical source models. Confer also to section 6.3.

The coefficients $\check{G}_n^0(\omega)$ describe the spatial transfer function of the employed secondary sources. These need not be modeled as a point source as it is commonly necessary in alternative approaches. In principle, any secondary source transfer function that does not exhibit zeros can be handled in the presented approach. However, the directivity characteristics have to be equal for all loudspeakers. Note that the coefficients $\check{G}_n^0(\omega)$ respectively $\check{G}_n^0(r, \omega)$ as used throughout this paper assume that the secondary

Table I. Expansion coefficients as defined by equation (5) for a selection of wave fields. (θ_{pw}, ϕ_{pw}) denotes the propagation direction of a plane wave, \mathbf{x}_s respectively (r_s, α_s, β_s) denote the position of a source. $h_n^{(2)}(\cdot)$ denotes the n -th order spherical Hankel function of second kind [10].

type	expansion coefficient $\check{P}_n^m(\omega)$
plane wave	$4\pi(-i)^n Y_n^m(\theta_{pw}, \phi_{pw})^*$
point source	$-i \frac{\omega}{c} h_n^{(2)}\left(\frac{\omega}{c}r_s\right) Y_n^m(\alpha_s, \beta_s)^*$
complex source	$\check{C}_n^m(\omega) \Lambda_n^m(\mathbf{x}_s)$ (see text)

source is situated at the position $(r = r_0, \alpha = 0, \beta = 0)$ and is orientated towards the coordinate origin. $\check{G}_n^0(r, \omega)$ can be yielded either from measurements or from analytical source models.

Equation (14) can be verified by inserting it into (9). After interchanging the order of integration and summation and exploitation of the orthogonality of the spherical harmonics, one arrives at the desired wave field, thus proving perfect reproduction. Note this is also true when the reproduced wave field is referenced to the center.

Since the coefficients $\check{P}_n^m(\omega)$ and $\check{G}_n^0(\omega)$ apparent in equation (14) are derived from interior expansions, (14) generally only holds for $|\mathbf{x}| < r_0$ [10].

4. Circular secondary source distributions

Sound field reproduction systems are frequently restricted to reproduction in the horizontal plane. The secondary sources are arranged on a circle. In this case, the acoustic scene to be reproduced as well as the receiver positions are bounded to the horizontal plane. In other words, the listener's ears have to be in the same plane like the secondary sources. For this two-dimensional setup the free-field Green's function required by the simple source approach can be interpreted as the spatial transfer function of a line source. This case is treated e.g. in [11, 21].

However, implementations of such systems usually employ loudspeakers with closed cabinets whose spatial transfer function is more accurately modeled by that of a point source. This secondary source type mismatch prevents us from perfectly recreating any source-free wave field inside the secondary source array. We have to expect artifacts. This circumstance is also a well treated problem in WFS [13]. The approach of employing secondary sources which are intended for three-dimensional reproduction in such an imperfect two-dimensional scenario is typically referred to as $2^{1/2}$ -dimensional reproduction.

The following derivation has been presented by the authors in [9].

4.1. Derivation of the driving function

For a circular distribution of secondary point sources, equation (9) degenerates to

$$P(\mathbf{x}, \omega) = \int_0^{2\pi} D(\alpha_0, \omega) \cdot G(\mathbf{x} - \mathbf{x}_0, \omega) r_0 d\alpha_0. \quad (15)$$

To bound our area of interest to the horizontal plane we set the elevation angle β in all position vectors to $\pi/2$ in the remainder of this section.

Equation (15) can be interpreted as a circular convolution and thus the convolution theorem [10]

$$\dot{P}_m(r, \omega) = 2\pi r_0 \dot{D}_m(\omega) \dot{G}_m(r, \omega) \quad (16)$$

and therefore

$$\dot{D}_m(\omega) = \frac{1}{2\pi r_0} \frac{\dot{P}_m(r, \omega)}{\dot{G}_m(r, \omega)} \quad (17)$$

featuring the Fourier series expansion coefficients $\dot{D}_m(\omega)$, $\dot{P}_m(r, \omega)$, and $\dot{G}_m(r, \omega)$ applies. Note that equation (16) only holds for two-dimensional wave fields. Since $\dot{P}_m(r, \omega)$ and $\dot{G}_m(r, \omega)$ are generally three-dimensional, (16) only holds in the horizontal plane (i.e. for $\beta = \pi/2$).

From equations (17) and (7) we can deduct that

$$D(\alpha, \omega) = \frac{1}{2\pi r_0} \sum_{m=-\infty}^{\infty} \frac{\dot{P}_m(r, \omega)}{\dot{G}_m(r, \omega)} e^{im\alpha}. \quad (18)$$

We reformulate the spherical harmonics expansion given by equation (4) by exchanging the order of summations to reveal the Fourier series expansion coefficients reading

$$F(r, \alpha, \beta = \frac{\pi}{2}, \omega) = \sum_{m=-\infty}^{\infty} e^{im\alpha} \cdot \underbrace{\sum_{n=|m|}^{\infty} \check{F}_n^m(\omega) j_n\left(\frac{\omega}{c}r\right) \sqrt{\frac{2n+1}{4\pi} \frac{(n-m)!}{(n+m)!}} P_n^m(0)}_{\dot{F}_m(r, \omega)}. \quad (19)$$

Introducing the explicit formulation of the Fourier series expansion coefficients $\dot{P}_m(r, \omega)$ and $\dot{G}_m(r, \omega)$ given by (19) into (18) yields the explicit driving function $D(\alpha, \omega)$. Analysis of the latter reveals that unlike the case of spherical secondary source distributions treated in section 3, the radius r does not cancel out. r appears both in the numerator as well as in the denominator in the summation over n in the argument of the spherical Bessel function $j_n\left(\frac{\omega}{c}r\right)$. The driving function is therefore dependent on the receiver position. This finding has already been derived in [6]. We thus have to reference the reproduced wave field to a specific radius which is then the only location where the reproduction is correct. Due to the complex mathematical structure of the numerator and the denominator in (18), the investigation of forbidden frequencies is not straightforward. We therefore propose to reference the reproduced wave field to the center of the secondary source array ($r = 0$) avoiding the formation of forbidden frequencies as described below.

At a first stage, setting $r = 0$ in (18) leads to an undefined expression of the form $\frac{0}{0}$ for $n \neq 0$ since spherical Bessel functions of argument 0 equal 0 $\forall n \neq 0$. Application of de l'Hôpital's rule [20] proves that the expression

is defined for $r = 0$ and finally yields the driving function $D_{2.5D}(\alpha, \omega)$ for 2^{1/2}-dimensional reproduction as

$$D_{2.5D}(\alpha, \omega) = \frac{1}{2\pi r_0} \sum_{m=-\infty}^{\infty} \frac{\check{P}_{|m|}^m(\omega)}{\check{G}_{|m|}^m(\omega)} e^{im\alpha}. \quad (20)$$

Note that the summation over n in (19) reduces to a single addend with $n = |m|$. Analogously to the reproduction using spherical secondary source arrays treated in section 3, equation (20) generally only holds for $|\mathbf{x}| < r_0$ due to the fact that the coefficients $\check{P}_{|m|}^m(\omega)$ and $\check{G}_{|m|}^m(\omega)$ are typically derived from interior expansions [10].

4.2. Reproduced wave field

We yield the actual wave field reproduced by the circular secondary source distribution by inserting (20) in (15) as

$$P_{2.5D}(\mathbf{x}, \omega) = \sum_{n=0}^{\infty} \sum_{m=-n}^n \check{P}_{|m|}^m(\omega) \frac{\check{G}_n^m(\omega)}{\check{G}_{|m|}^m(\omega)} \cdot j_n\left(\frac{\omega}{c}r\right) Y_n^m(\alpha, \beta) \quad \forall r < r_0. \quad (21)$$

Note that $\check{P}_{|m|}^m(\omega)$ are the coefficients of the desired wave field.

Figures 2a and 2b show the real part and the absolute value of the sound pressure $P_{2.5D, pw}(\mathbf{x}, \omega)$ of a continuous circular secondary monopole distribution with $r_0 = 1.5$ m reproducing a virtual plane wave of $f_{pw} = 1000$ Hz with propagation direction $\theta_{pw} = 3\pi/2$. The angular bandwidth of the driving function was limited to $n_{max} = 40$ for the simulation. The analytical expression for $P_{2.5D, pw}(\mathbf{x}, \omega)$ is yielded by inserting the appropriate coefficients listed in Table I into (21).

From Figure 2a it can be seen that the wave fronts of $P_{2.5D, pw}(\mathbf{x}, \omega)$ are indeed perfectly plane. Though, an amplitude decay of approximately 3dB per doubling of the distance is apparent when following the propagation path of the plane wave. Figure 2b further illustrates this amplitude decay by depicting the absolute value of the sound pressure in logarithmic scale. This inherent amplitude error is also known from WFS [22].

Further investigation of the reproduced wave field reveals that subtle spectral alterations are present.

5. Discretization of the secondary source distribution

For the theoretic continuous spherical secondary source distribution, any wave field which is source-free inside the secondary source distribution can be perfectly reproduced apart from the forbidden frequencies. The properties of the continuous circular secondary source distribution are discussed in section 4.2.

Real-world implementations of audio reproduction systems will always employ a limited number of discrete secondary sources. The spatial discretization constitutes spatial sampling and thus may produce spatial aliasing. In this section, we discuss the consequences of spatial sampling.

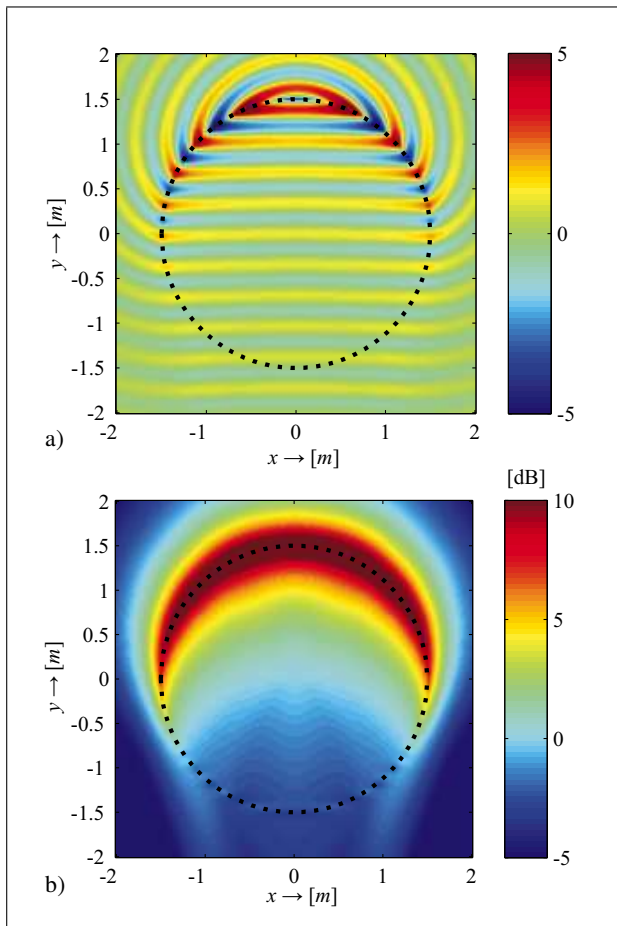


Figure 2. Sound pressure $P_{2.5D,pw}(\mathbf{x}, \omega)$ of a continuous circular distribution with radius $r_0 = 1.5$ m of secondary monopole sources reproducing a virtual plane wave of $f_{pw} = 1000$ Hz and unit amplitude with propagation direction $\theta_{pw} = 3\pi/2$ referenced to the coordinate origin. The secondary source distribution is indicated by the dotted line. The wave field outside the secondary source distribution was derived via the according exterior expansions [10]. a) $\Re\{P_{2.5D,pw}(\mathbf{x}, \omega)\}$, b) $20 \cdot \log_{10} |P_{2.5D,pw}(\mathbf{x}, \omega)|$.

For convenience, we exemplarily consider two-dimensional reproduction. It was shown in section 4.2, that amplitude errors emerge from using point-like sources as secondary sources for two-dimensional reproduction. It was already noted in section 4 that line sources are the appropriate choice as secondary sources for this case. In order to purely investigate the consequences of spatial sampling without additional amplitude errors, we will use line sources as secondary sources in the following. The derived results also hold qualitatively for point sources as secondary sources.

Due to the fact that the driving functions presented in this paper are generally valid only inside the secondary source distribution, we only consider artifacts that arise ibidem.

5.1. Spatial sampling artifacts

We consider a circular secondary line source distribution which is sampled equi-angularly due to the practical rele-

vance of this setup. We follow the methodology developed in [13, 23].

The discretization of the secondary source distribution can be conveniently modeled by an angular sampling of the continuous driving function

$$D_S(\alpha, \omega) = D(\alpha, \omega) \sum_{l=0}^{L-1} \delta(\alpha - \frac{l}{L} 2\pi), \quad (22)$$

whereby L denotes the total number of sampling points (i.e. loudspeakers). It can be shown that the angular sampling of the driving function results in repetitions of the angular spectrum

$$\hat{D}_{m,S}(\omega) = \sum_{\mu=-\infty}^{\infty} \hat{D}_{m+\mu L}(\omega). \quad (23)$$

The reproduced wave field for a spatially sampled secondary source distribution is given by introducing (23) into (16). Hence, the spatially sampled driving function $\hat{D}_{m,S}(\omega)$ is weighted by the angular spectrum of the secondary sources. In the context of sampling, the secondary sources can be regarded as spatial interpolators from the boundary into the listening area.

The formation of spatial sampling artifacts depends on the bandwidth of the angular spectrum of the driving function $D(\alpha, \omega)$ and the secondary sources $G(\mathbf{x} - \mathbf{x}_0, \omega)$. The wave field of a secondary line source situated at \mathbf{x}_0 is given as [10]

$$G(\mathbf{x} - \mathbf{x}_0, \omega) = \frac{i}{4} H_0^{(2)}(k |\mathbf{x} - \mathbf{x}_0|), \quad (24)$$

where $H_0^{(2)}(\cdot)$ denotes the zeroth-order Hankel function of second kind.

The angular spectrum of the secondary sources can be derived by applying the shift theorem of the Hankel functions [24] to (24) for $\alpha_0 = 0$ as

$$\hat{G}_m(r, \omega) = \frac{i}{4} J_m\left(\frac{\omega}{c} r\right) H_m^{(2)}\left(\frac{\omega}{c} r_0\right) \quad \forall m, \quad (25)$$

whereby $J_m(\cdot)$ denotes the m -th order Bessel function. $\hat{G}_m(r, \omega)$ is thus not bandlimited with respect to the angular frequency m .

For alias-free reproduction $\hat{D}_m(\omega)$ has to be bandlimited with respect to the angular frequency m such that the repetitions introduced due to sampling do not overlap (confer to equation 23). For entirely artifact-free reproduction $\hat{G}_m(r, \omega)$ also has to be bandlimited in order to suppress the spectral repetitions of the sampled driving function. Since especially the latter is not the case, artifact-free reproduction is in general not possible using circular arrays of secondary monopoles. Note that when the repetitions of the angular spectrum of $D(\alpha, \omega)$ do not overlap, the reproduction is aliasing-free. The artifacts due to spatial discretization in this case are rather a consequence of the inappropriate reconstruction filter $\hat{G}_m(r, \omega)$ which does not suppress the spectral repetitions of the driving function. However, this type of reconstruction error is typically also

referred to as *spatial aliasing* and we therefore do so as well in the remainder of this paper.

Due to the weighting of the angular spectrum of the driving function by with the angular spectrum of the secondary sources, spatial sampling artifacts will be more prominent for higher frequencies. This follows directly from the properties of the involved Bessel and Hankel functions.

As noted above, it is desirable that the angular spectrum of $D(\alpha, \omega)$ is bandlimited in order to prevent spectral overlapping. The maximum angular bandwidth doing so is a bandwidth of one repetition of the sampled driving function $\hat{D}_{m,S}(\omega)$, thus

$$D(\alpha, \omega) = \frac{1}{2\pi r_0} \sum_{m=-M}^M \hat{D}_m(\omega) e^{im\alpha}, \quad (26)$$

with $M = (L-1)/2$ for odd L and accordingly for even L . This results in a sampled driving function $D_S(\alpha, \omega)$ reading

$$D_S(\alpha, \omega) = \frac{1}{2\pi r_0} \sum_{m=-M}^M \sum_{\mu=-\infty}^{\infty} \hat{D}_m(\omega) e^{i(m+\mu L)\alpha}. \quad (27)$$

In order to quantify the spatial sampling artifacts a specific desired wave field has to be considered. Since arbitrary wave fields can be decomposed into plane waves [10], a plane wave is exemplarily chosen as desired wave field in the following. The angular spectrum of a plane wave with incidence angle θ_{pw} reads

$$\hat{P}_{m,pw}(r, \omega) = i^{-m} J_m\left(\frac{\omega}{c} r\right) e^{-im\theta_{pw}}. \quad (28)$$

The continuous driving function $D_{pw}(\alpha, \omega)$ is given by introducing (28) and (25) into (26) as

$$D_{pw}(\alpha, \omega) = \frac{1}{2\pi r_0} \sum_{m=-M}^M \underbrace{(-4i) \frac{i^{-m} e^{-im\theta_{pw}}}{H_m^{(2)}\left(\frac{\omega}{c} r_0\right)}}_{=\hat{D}_{m,pw}(\omega)} e^{im\alpha}. \quad (29)$$

The sampled driving function $D_{S,pw}(\alpha, \omega)$ is yielded by adopting (29) to (27). Note that in (29) the reproduced wave field is referenced to the center of the secondary source distribution in order to avoid the formation of forbidden frequencies (confer also to section 3).

The reproduced wave field for a spatially discrete secondary source distribution is then

$$P_{S,pw}(\mathbf{x}, \omega) = \sum_{m=-M}^M \sum_{\mu=-\infty}^{\infty} e^{i(m+\mu L)\alpha} \cdot \frac{i^{-m} e^{-im\theta_{pw}}}{H_m^{(2)}\left(\frac{\omega}{c} r\right)} J_{m+\mu L}\left(\frac{\omega}{c} r\right) H_{m+\mu L}^{(2)}\left(\frac{\omega}{c} r_0\right). \quad (30)$$

For $\mu = 0$, (30) represents the bandlimited desired wave field, the terms for $\mu \neq 0$ represent spatial sampling artifacts. From (30) it can be deduced that spatial sampling

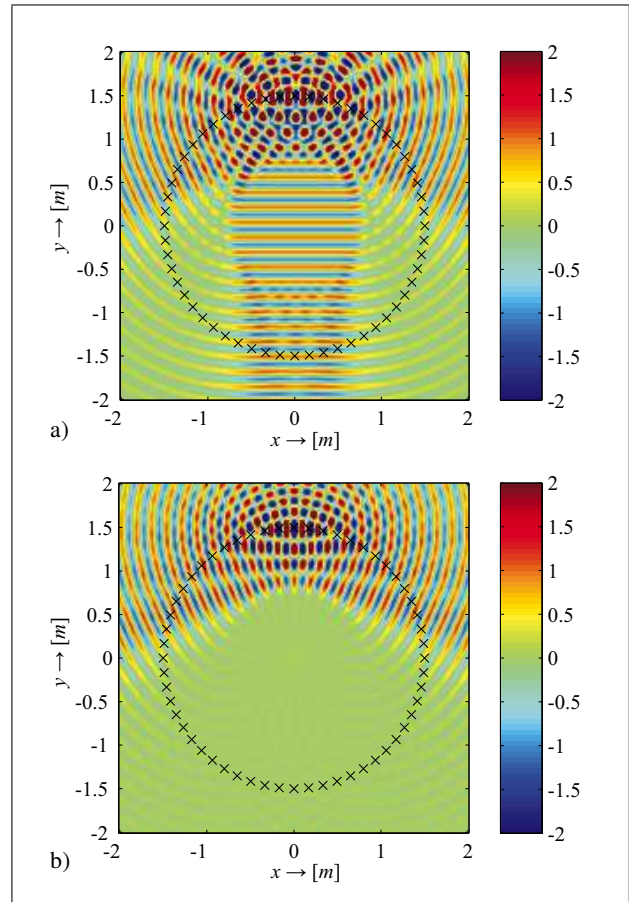


Figure 3. Reproduced wave field $P_{S,pw}(\mathbf{x}, \omega)$ and its spatial sampling artifacts for a discrete circular distribution of $L = 56$ secondary line sources with a radius of $r_0 = 1.5$ m when reproducing monochromatic plane wave of $f_{pw} = 2000$ Hz and propagation direction $\theta_{pw} = 3\pi/2$. 3 repetitions of the angular spectrum are considered. a) Reproduced wave field, b) Spatial sampling artifacts.

artifacts constitute a distortion of the spatial structure of the reproduced wave field.

The effects of spatial sampling will be illustrated in the following for a particular reproduction setup. The geometrical parameters are chosen in accordance to the loudspeaker system installed at the Usability Laboratory of Deutsche Telekom Laboratories. Figure 3 illustrates the reproduced wave field and its spatial sampling artifacts for a circular system with $N = 56$ secondary line sources placed on a circular contour with a radius of $r_0 = 1.5$ m. The desired wave field is a monochromatic plane wave of $f_{pw} = 2000$ Hz with propagation direction $\theta_{pw} = 3\pi/2$. The reproduced wave field without spatial sampling artifacts is depicted in Figure 5b.

In order to illustrate the spatial energy distribution of the spatial sampling artifacts we additionally computed the reproduced aliasing-to-signal ratio (RASR). The RASR is defined as the energy ratio of the reproduced aliasing contributions (respectively the spatial sampling artifacts) and the desired wave field [23] with varying (temporal) bandwidth of the reproduced wave field. Note that the percep-

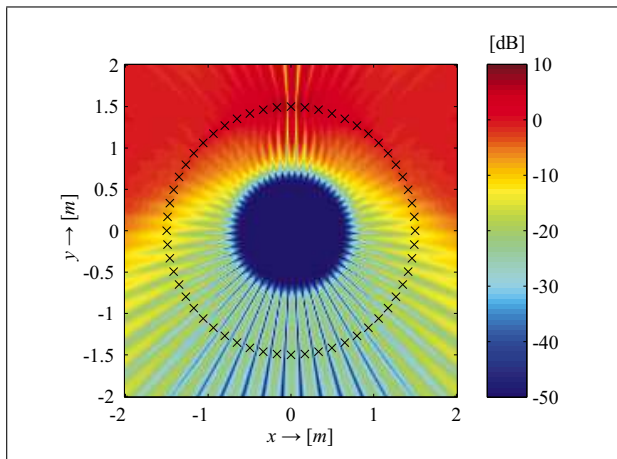


Figure 4. Reproduced aliasing-to-signal ratio (RASR) for the wave field shown in Figure 3. The considered frequency range is 0 – 2000 Hz. The values are clipped as indicated by the color-bar.

tual relevance of the RASR is not clear. We use it due to the lack of an alternative.

In general, the RASR will depend on the desired wave field and the receiver position. The RASR is zero ($-\infty$ dB) for artifact-free reproduction. Figure 4 shows the RASR for the above described reproduction scenario. In this case, the considered frequency range is 0–2000 Hz.

The presented results show that the RASR depends on the receiver position: The closer the receiver position is to the center of the secondary source array, the lower is the energy of the spatial sampling artifacts. Further investigation of the RASR reveals that the higher the temporal bandwidth of the plane wave is, the more energy is contained in the spatial sampling artifacts of the reproduced field and the smaller gets the disc around the center where only low artifacts are apparent for a given frequency range.

The spatial sampling artifacts are illustrated in Figure 3b. For the relatively low frequency of 2000 Hz already a considerable amount of aliasing occurs. The amount of aliasing increases further with the frequency. Since a closer loudspeaker spacing (and therefore preferable spatial sampling properties) than simulated is hardly feasible in practical implementations, it has to be noted that sound reproduction in the full audible bandwidth (far beyond 15 kHz) can not be accurately accomplished due to severe spatial sampling artifacts. There are indications that the human ear is not very sensitive towards this type of artifacts when stationary situations are considered. Results obtained in the context of wave field synthesis show that spatial aliasing artifacts are perceived as a rather subtle though audible timbral coloration [25]. However, it is not clear how this perceived coloration is related to the RASR and therefore no conclusion can be drawn from Figure 4 at this stage.

5.2. Truncation error

In this section, we investigate the consequences that the truncation of the spatial bandwidth of the driving func-

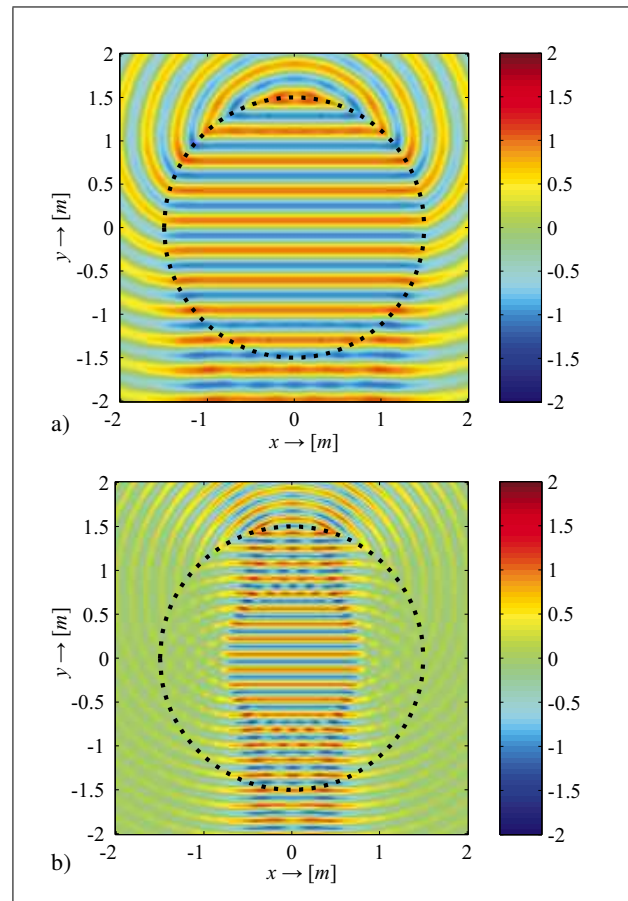


Figure 5. Wave fields reproduced by a continuous circular distribution of secondary line sources with a radius of $r_0 = 1.5$ m when reproducing a monochromatic plane wave with propagation direction $\theta_{pw} = \frac{3\pi}{2}$. The spatial bandwidth of the driving functions and therefore of the reproduced wave field is limited to the interval $[-27; 27]$. The secondary source distribution is indicated by the dotted line. a) $f_{pw} = 1000$ Hz, b) $f_{pw} = 2000$ Hz.

tion introduced in (26) implies. Note that the findings in this section are derived independently from spatial sampling artifacts. For discrete loudspeaker setups, both artifacts combine. For convenience, we stay in two dimensions. An extension of the following derivation to three dimensions can be found in [26].

Rewriting (7), we yield

$$P(\mathbf{x}, \omega) = \sum_{m=-\infty}^{\infty} \check{P}_m(\omega) J_m\left(\frac{\omega}{c} r\right) e^{im\alpha} \quad (31)$$

as Fourier series expansion of a two-dimensional wave field [10].

The normalized field truncation error as defined in [26] reads

$$\epsilon_N(r_0, \omega) = \frac{1}{\pi r_0^2} \int_0^{r_0} \int_0^{2\pi} \frac{|P(\mathbf{x}, \omega) - P_M(\mathbf{x}, \omega)|}{|\bar{P}(\omega)|} d\alpha r dr. \quad (32)$$

$P(\mathbf{x}, \omega)$ denotes a wave field with full angular bandwidth as given in (31), $P_M(\mathbf{x}, \omega)$ is the same wave field

whereby the expansion orders m are confined to the interval $[-M; M]$. As suggested by (26), M should be chosen equal to or smaller than $(L - 1)/2$ for odd numbers of loudspeakers L and accordingly for even numbers in order to prevent overlapping in the angular spectrum when a discrete loudspeaker setup is considered.

The normalization in (32) takes place with respect to the absolute value of the plane wave expansion $|\bar{P}(\omega)|$ of the full-bandwidth wave field at $r = 0$ integrated along the unit circle. Note that for plane waves with unit amplitude $\bar{P}(\omega) = 1$.

It can be shown that

$$\frac{|P(\mathbf{x}, \omega) - P_M(\mathbf{x}, \omega)|}{|\bar{P}(\omega)|} \leq \eta e^{-\Delta} \quad (33)$$

holds for the integrand in (32), provided that the truncation order is chosen as [26]

$$M = \left\lceil \frac{er\omega}{2c} \right\rceil + \Delta. \quad (34)$$

In the above, $\eta \approx 0.16127$, Δ is an integer and equal to or larger than 0, and $\lceil \cdot \rceil$ denotes the integer ceiling function.

Equations (33) and (34) state that the upper bound of the relative truncation error is 16.1% once M equals the critical threshold $\lceil er\omega/2c \rceil$. For higher M , the relative truncation error decreases at least exponentially as M increases [26].

For sound field reproduction purposes, this implies that a minimum truncation order and thus implicitly a minimum number of loudspeakers can be determined for a given frequency ω and a given disc of radius r , above which the relative truncation error decreases at least exponentially as the number of loudspeakers and the truncation order are increased. In order to determine guidelines for the design of sound field reproduction systems, the remaining question to be answered is which amount of truncation error is tolerated by the human ear without making the perception distinguishable from full spatial bandwidth.

For the setup from Figure 3, i.e. $r_0 = 1.5$ m and $L = 56$, the frequency up to which (34) is fulfilled is approximately 700 Hz. Recall that the entire audible bandwidth significantly exceeds 15 kHz. Therefore, severe truncation errors have to be expected for a loudspeaker setup comparable to the one considered here.

A fundamental property of the truncation error to note is its dependency both on the frequency as well as on the receiver position. This circumstance is illustrated in Figure 5 for a continuous circular distribution of secondary line sources with a radius of $r_0 = 1.5$ m when reproducing monochromatic plane waves of different frequencies. The spatial bandwidth of the driving functions and therefore of the reproduced wave field is limited to the interval $[-27; 27]$. It can be seen that a consequence of truncation of the spatial bandwidth is the fact that the region of accurate reproduction concentrates around the center of the array with increasing frequency. In certain locations outside the region of accurate reproduction the amplitude of the

reproduced wave field is relatively low. This follows directly from the properties of the involved Bessel and Hankel functions.

In other words, for broadband signals higher temporal frequencies are significantly attenuated with increasing distance of the receiver position from the center of the array in some directions. Thus, the sound color of the reproduced wave field drastically changes.

6. Rendering techniques

6.1. Model-based reproduction

In model-based reproduction *virtual* acoustic scenes are reproduced. The involved wave fields are described analytically. Table I gives a brief summary of the most common employed source models. Of course, the source models apply both to the virtual as well as to the secondary sources.

Table I also features the expansion coefficients $\check{C}_n^m(\omega)$ $\Lambda_n^m(\mathbf{x}_s)$ of virtual complex sources. These complex sources can be both directional and/or spatially extended sources. Their spatio-temporal transfer function is typically described by the expansion coefficients $\check{C}_n^m(\omega)$ assuming that the source is situated in the origin of the coordinate system. In order to yield the expansion coefficients of an arbitrary source position \mathbf{x}_s , appropriate translation and rotation of the coefficients have to be applied. This operation is indicated in Table I by the operator $\Lambda_n^m(\mathbf{x}_s)$. Details can be found in [27].

Note that an alternative approach to the reproduction of virtual complex sources is presented in [28]. However, this approach is rather pragmatic and is per se an approximation. We are therefore in favor of consequently staying in the presented framework and describing virtual complex sources as indicated in Table I.

A special situation arises when a virtual sound source is positioned inside the secondary source distribution. The properties of the virtual source's wave field make it impossible to reproduce the wave field correctly over the entire listening area [29]. The reproduced wave field is only correct inside a sphere resp. a disc with a radius equal to the distance of the virtual source from the coordinate origin. Outside this sphere/disc, severe degradations of the wave field occur, most notably a strong boost of low frequencies [29]. In this situation, it is favorable not to reproduce a virtual source but a focused wave field [30]. This focused wave field then exhibits the far-field radiation characteristics of the intended virtual source in one half space. This half space can be freely chosen with the only restriction that its boundary has to contain the intended virtual source's position. See [30] for details.

6.2. Data-based reproduction

The reproduction capabilities of the presented approach (as those of the alternative approaches) are not restricted to virtual sound sources. Appropriately captured wave fields can be recreated as well. In the latter case, the desired wave

field is described by the expansion coefficients of the captured one. A thorough treatment of the properties and limitations of the capturing approaches can be found e.g. in [4, 31].

The accurate capturing of a sound field requires the synthesis of higher microphone directivities than are available from traditional first order microphones. This can be accomplished by employing microphone arrays. Due to the secondary source geometry considered here, spherical microphone arrangements are the most preferable choice. They can provide equal properties for all angles of sound incidence. The spherical wave spectrum of the captured sound field (confer to (35)) and therefore its spatial encoding can be obtained from the microphone signals. However, due to current practical limitations, only a few lower order expansion coefficients can be obtained.

6.3. Spatial en-/decoding

The spatial wave field encoding and decoding procedure outlined in this section was introduced in the context of Ambisonics [2]. The encoding procedure yields a representation of a sound scene which is independent from the loudspeaker geometry and allows for the storage and transmission of the sound scene. The decoding procedure yields the loudspeaker driving signals for an encoded scene for a given loudspeaker distribution. Note that both model-based and data-based sound scenes can be encoded.

A wave field to be reproduced can be spatially encoded when it is known on a sphere with radius r_{ref} and when the number of its expansion coefficients is limited:

$$P(r = r_{\text{ref}}, \alpha, \beta, \omega) = \sum_{n=0}^N \sum_{m=-n}^n \hat{P}_n^m(r_{\text{ref}}, \omega) Y_n^m(\alpha, \beta). \quad (35)$$

$P(\mathbf{x}, \omega)$ has to be free of sound sources for $r < r_{\text{ref}}$. The correspondences of the coefficients $\hat{P}_n^m(r_{\text{ref}}, \omega)$ in the time domain are termed *Ambisonics signals* and can be stored and transmitted [32]. Note that $\hat{P}_n^m(r_{\text{ref}}, \omega)$ is also referred to as spherical wave spectrum [10].

It is not advisable to store the coefficients $\hat{P}_n^m(\omega)$ (confer to (5)), since they diverge at low frequencies for all expansion orders $n \neq 0$ [29]. When the reference radius r_{ref} is considered in the decoding process as

$$D(\alpha, \beta, \omega) = \frac{1}{2\pi r_0} \sum_{n=0}^N \sum_{m=-n}^n \sqrt{\frac{2n+1}{4\pi}} \frac{\hat{P}_n^m(r_{\text{ref}}, \omega)}{\hat{G}_n^0(\omega) j(kr_{\text{ref}})} Y_n^m(\alpha, \beta) \quad (36)$$

exemplarily with a spherical array, the reproduction can be properly accomplished.

In certain situations, the involved wave field expansions have limited validity. When $\hat{G}_n^0(r_G, \omega)$ is valid on the surface of a sphere with radius r_G , $\hat{P}_n^m(r_{\text{ref}}, \omega)$ has to be extrapolated to $\hat{P}_n^m(r_G, \omega)$ as [10]

$$\hat{P}_n^m(r_G, \omega) = \frac{j_n\left(\frac{\omega}{c} r_G\right)}{j_n\left(\frac{\omega}{c} r_{\text{ref}}\right)} \hat{P}_n^m(r_{\text{ref}}, \omega). \quad (37)$$

The reproduced wave field is then per se only accurate inside the sphere respectively the disc with a radius equal to the smaller of r_{ref} and r_G . Note that the zeros arising in the denominator in (37) limit its applicability [10].

Inside this sphere, the encoded wave field may not contain sound sources. The extrapolation in forward direction, i.e. when r_G respectively r_0 are smaller than r_{ref} , does not pose further theoretical restrictions. When r_G resp. r_0 is larger than r_{ref} , the description of the captured wave field has to be extrapolated in backward direction to r_0 resp. r_G . This does not pose theoretical restrictions either as long as the encoded wave field does not contain sound sources (direct ones or indirect ones like reflecting bodies) inside the sphere with radius r_0 resp. r_G . If it does so, the same issues arise as with the reproduction of virtual sound sources inside the secondary source array described in section 6.1.

6.4. Plane waves as secondary source wave fields

A special type of driving function arises when the loudspeakers are arranged on a circle and are assumed to be far enough away from the center of the array, that their sound fields can be modeled as plane waves there. If a virtual plane wave is intended to be reproduced, then the driving functions are simple amplitude weights. In that case, no delaying or spectral filtering of the audio signals is necessary. This procedure is the basic Ambisonics approach proposed by Gerzon e.g. in [33].

Note however that the reproduced wave field strongly departs from the desired plane wave when the receiver moves away from the center of the array. Even there, the wave field exhibits a considerable curvature for typical radii of loudspeaker arrangements of a few meters. The reproduced wave field appears to originate from a point source situated on the contour of the loudspeaker array [29]. Especially for systems employing a large number of loudspeakers and driving functions that include high expansion orders, the vast part of the energy of the driving function is concentrated in the vicinity of the resulting virtual point-like source.

Confer to Figure 6. It depicts the wave field $P(\mathbf{x}, \omega)$ reproduced by the loudspeaker system from Figure 3 driven by the appropriate amplitude panning driving functions, i.e. weights.

The extension of the traditional Ambisonics approach which models the loudspeakers' sound fields as finite distance sources has been termed *near-field compensated Ambisonics* [29]. Here, the term *near-field* describes the sound field of any source which is closer to the point of observation than infinity.

7. Conclusions

In this paper, a comprehensive treatment of sound field reproduction using circular and spherical loudspeaker distributions was presented. The formulation of the approach assumes a continuous distribution of secondary sources on which sampling is performed to yield the actual loudspeaker driving signals for a given loudspeaker setup.

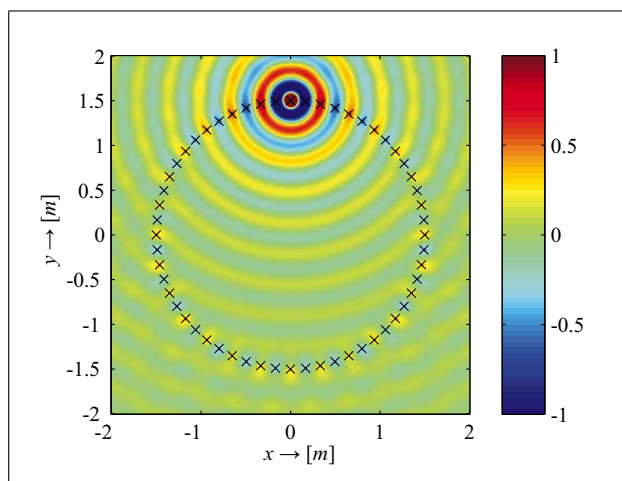


Figure 6. $\Re\{P(\mathbf{x}, \omega)\}$ of a circular distribution with radius $r_0 = 1.5$ m of 56 secondary monopole point sources reproducing the virtual plane wave from Figure 2 but using the amplitude panning driving function. The marks indicate the secondary source positions.

This strategy enables an analytical derivation of the loudspeaker driving signals and thus also of the reproduced wave field which facilitates the investigation of the properties of the latter. In the case of a volume enclosed by the secondary source distribution, the formulation lead directly to the simple source approach, thus providing the physical justification for the presented approach to recreate arbitrary source-free wave fields. Circular secondary source arrangements impose artifacts on the reproduced wave field, notably an incorrect amplitude decay and subtle spectral alterations. The reproduced wave field is then only correct in the center of the loudspeaker array.

We presented a detailed treatment of both application alternatives, i.e. model-based and data-based reproduction (the reproduction of virtual respectively captured sound scenes). In the case of the virtual scenes, strategies to handle arbitrary virtual source types, notably point sources, plane sources, and complex (i.e. directional and spatially extended) sources were presented. In the case of the reproduction of captured sound scenes, a introduction to recording approaches was given as well as a description of the procedure of processing a recording in order to adapt it to a given loudspeaker setup.

Contrary to most common approaches, the reproduction is not limited to the employment of secondary monopole sources.

The entirely analytical property of the presented approach facilitates the investigation of the consequences of an insufficient loudspeaker layout which occurs in real world implementations (e.g. spatial sampling). Furthermore, costly numerical algorithms (as e.g. in [3, 7, 5, 6, 8]) are avoided. Although not proven so far, the present approach can be assumed to be significantly beneficial in terms of the involved computational complexity. Firstly, the procedure to find the driving functions can be assumed to be more efficient in the analytical approach presented

here. And secondly, in model-based reproduction a pure delay can be extracted from the secondary source driving function [34]. This is not the case in numerical methods resulting in significantly longer filters.

Finally, there are no stability issues for incomplete loudspeaker setups as in the traditional approach.

References

- [1] A. J. Berkhout, D. de Vries, P. Vogel: Acoustic control by wave field synthesis. *J. Acoust. Soc. Am.* **93** (May 1993) 2764–2778.
- [2] M. A. Gerzon: With-height sound reproduction. *J. Audio Eng. Soc.* **21** (1973) 2–10.
- [3] J. Daniel: Représentation de champs acoustiques, application à la transmission et à la reproduction de scènes sonores complexes dans un contexte multimédia. PhD thesis Université Paris 6, 2001.
- [4] B. Rafaely: Analysis and design of spherical microphone arrays. *IEEE Trans. On Sp. and Audio Proc.* **13** (Jan. 2005) 135–143.
- [5] O. Kirkeby, P. A. Nelson: Reproduction of plane wave sound fields. *J. Acoust. Soc. Am.* **94** (Nov. 1993) 2992–3000.
- [6] D. B. Ward, T. D. Abhayapala: Reproduction of a plane-wave sound field using an array of loudspeakers. *IEEE Trans. on Sp. and Audio Proc.* **9** (Sep. 2001) 697–707.
- [7] M. A. Poletti: Three-dimensional surround sound systems based on spherical harmonics. *J. Audio Eng. Soc.* **53** (Nov. 2005) 1004–1025.
- [8] J. Hannemann, K. D. Donohue: Virtual sound source rendering using a multipole-expansion and method-of-moments approach. *J. Audio Eng. Soc.* **56** (June 2008) 473–481.
- [9] J. Ahrens, S. Spors: Analytical driving functions for higher order ambisonics. *IEEE International Conference on Acoustics, Speech and Signal Processing (ICASSP)*, Las Vegas, Nevada, March 30th–April 4th 2008.
- [10] E. G. Williams: *Fourier acoustics: Sound radiation and nearfield acoustic holography*. Academic Press, London, 1999.
- [11] Y. J. Wu, T. D. Abhayapala: Soundfield reproduction using theoretical continuous loudspeaker. *IEEE International Conference on Acoustics, Speech and Signal Processing (ICASSP)*, Las Vegas, Nevada, March 30th–April 4th 2008.
- [12] R. Nicol: *Restitution sonore spatialisée sur une zone étendue: application à la téléprésence*. PhD thesis Université du Maine, Le Mans, 1999.
- [13] S. Spors, J. Ahrens: A comparison of wave field synthesis and higher-order ambisonics with respect to physical properties and spatial sampling. *125th Convention of the AES*, San Francisco, CA, Oct. 2–5 2008.
- [14] F. Fazi, P. Nelson: A theoretical study of sound field reconstruction techniques. *19th International Congress on Acoustics*, Madrid, Spain, Sept. 2–7 2007.
- [15] B. Girod, R. Rabenstein, A. Stenger: *Signals and systems*. J. Wiley & Sons, 2001.
- [16] Wikipedia: Ambisonics — Wikipedia, The Free Encyclopedia. 2008. [Online; accessed 28-Feb-2008].

- [17] J. Ahrens, S. Spors: Reproduction of a plane-wave sound field using planar and linear arrays of loudspeakers. *IEEE Int. Symp. on Comm., Control and Sig. Proc. (ISCCSP)*, Malta, March 12th–14th 2008.
- [18] L. G. Copley: Fundamental results concerning integral representations in acoustic radiation. *J. Acoust. Soc. Am.* **44** (1968) 28–32.
- [19] J. R. Driscoll, D. M. Healy: Computing fourier transforms and convolutions on the 2-sphere. *Advances in Applied Mathematics* **15** (June 1994) 202–250.
- [20] E. W. Weisstein: L'Hospital's Rule. *MathWorld – A Wolfram Web Resource*. <http://mathworld.wolfram.com/LHospitalsRule.html>, retrieved Jan. 08.
- [21] M. A. Poletti: A unified theory of horizontal holographic sound systems. *J. Audio Eng. Soc.* **48** (Dec. 2000) 1155–1182.
- [22] J.-J. Sonke, J. Labeeuw, D. de Vries: Variable acoustics by wavefield synthesis: A closer look at amplitude effects. 104th Convention of the AES, Amsterdam, The Netherlands, May 16–19 1998.
- [23] S. Spors, R. Rabenstein: Spatial aliasing artifacts produced by linear and circular loudspeaker arrays used for wave field synthesis. 120th Convention of the AES, Paris, France, May 20–23 2006.
- [24] M. Abramowitz, I. A. Stegun (eds.): *Handbook of mathematical functions*. Dover Publications Inc., New York, 1968.
- [25] H. Wittek: Perceptual differences between wavefield synthesis and stereophony. PhD thesis, University of Surrey, 2007.
- [26] R. A. Kennedy, P. Sadeghi, T. D. Abhayapala, H. M. Jones: Intrinsic limits of dimensionality and richness in random multipath fields. *IEEE Trans. on Sig. Proc.* **55** (June 2007) 2542–2556.
- [27] N. A. Gumerov, R. Duraiswami: *Fast multipole methods for the Helmholtz equation in three dimensions*. Elsevier, Amsterdam, 2004.
- [28] D. Menzies: Ambisonic synthesis of complex sources. *J. Audio Eng. Soc.* **55** (Oct. 2007) 864–876.
- [29] J. Daniel: Spatial sound encoding including near field effect: Introducing distance coding filters and a viable, new ambisonic format. 23rd International Conference of the AES, Copenhagen, Denmark, May 23–25 2003.
- [30] J. Ahrens, S. Spors: Focusing of virtual sound sources in higher order ambisonics. 124th Convention of the AES, Amsterdam, The Netherlands, May 17–20 2008.
- [31] J. Meyer, G. W. Elko: Spherical microphone arrays for 3D sound recording. In Y. Huang and J. Benesty, *Audio Signal Processing for Next-Generation Multimedia Communication Systems*, Kluwer Academic Publishers, 2004.
- [32] R. Rabenstein, S. Spors: Multichannel sound field reproduction. In Benesty, J., Sondhi, M., Huang, Y. (Eds.), *Springer Handbook on Speech Processing and Speech Communication*, Springer Verlag, 2007.
- [33] M. Gerzon: Ambisonics in multichannel broadcasting and video. *J. Audio Eng. Soc.* **33** (Nov. 1985) 859–871.
- [34] F. Zotter, M. Noisternig: Near- and farfield beamforming using spherical loudspeaker arrays. 3rd Congress of the Alps Adria Acoustics Association, Graz, Austria, Sept. 27th–28th 2007.